Genet. Sel. Evol. 33 (Suppl. 1) (2001) S85 S104



**Original article**

# Numerical simulation for freezing and thawing mammalian spermatozoa. Evaluation of cell injuries at different depths in bags or straws during all steps of the technique

Jean-Luc COURTENS[a,*], Jean-Michel RÉTY[b]

[a] Institut national de la recherche agronomique, 37380 Nouzilly, France
[b] Lore, 11 boulevard Pershing, 75017 Paris, France

**Abstract** – A numerical simulation of freezing-thawing protocols applicable to mammalian spermatozoa is described and validated in the boar and the ram. Original aspects include: (1) the simulation of all steps of the technique from ejaculation to thawing, (2) the simulation of complex extenders really usable in field conditions and extender properties in non-ideal conditions, (3) the sequential extender changes within a protocol for simulation of dilutions, additions, etc. (4) the introduction of a new concept, the "molecular chicanes" which reconciles theoretical and experimental results, (5) the introduction of specific cell models and (6) the prediction of different cell injuries at various depths in flat and cylindrical plastic cryocontainers. The calculated data indicate when, where and why cells are affected during each step of the technique and can therefore help to increase the total number of living spermatozoa or to devise new techniques rapidly. For validation, calculated data are compared to experimental and literature results. In boars and rams, simulations and observations generally differ by less than 5%.

**numerical simulation / freezing-thawing / mammalian spermatozoa / ram / boar**

**Résumé – Simulation numérique de cryoconservation des spermatozoïdes de mammifères. Prédiction des atteintes cellulaires à différentes profondeurs de sacs ou de paillettes au cours de toutes les étapes de la technique.** Une simulation numérique de cryoconservation des spermatozoïdes de mammifères est décrite et validée chez le Bélier et le Verrat. Elle inclue des aspects originaux : (1) la simulation de toutes les étapes de la technique, de l'éjaculation au dégel, (2) la prise en compte des solutions non-idéales et de dilueurs complexes réellement utilisables sur le terrain, (3) la possibilité de les modifier en cours de simulation,

* Correspondence and reprints
E-mail: courtens@tours.inra.fr

pour mimer les dilutions successives, ajouts, etc., (4) l'introduction du nouveau concept de « chicane moléculaire » qui réconcilie résultats théoriques et pratiques, (5) la définition de modèles cellulaires spécifiques et (6) la prédiction des altérations cellulaires à différentes profondeurs dans les cryocontainers plats ou cylindriques. Les calculs indiquent quand, où et pourquoi les cellules sont altérées et peuvent de ce fait être utilisés pour améliorer le nombre total de spermatozoïdes vivants, ou évaluer rapidement une technique nouvelle. La validation s'appuie sur une comparaison entre résultats calculés et résultats expérimentaux ou publiés par d'autres auteurs. Chez le Verrat et le Bélier, simulations et viabilités réelles diffèrent généralement de moins de 5 %.

**simulation numérique / congélation-décongélation / spermatozoïdes de mammifères / bélier / verrat**

## Symbols and abbreviations used in formulas

| | |
|---|---|
| $c$ | : Solution specific heat (J/$\mu$g/K). |
| $c_i$ | : Concentration of the solute $i$ ($\mu$g/mm$^3$). |
| $D_i$ | : Diffusivity coefficient of the solute $i$ (mm$^2$/s). |
| $Ea$ | : Activation energy (J/mol). |
| $L$ | : Water heat of fusion (J/$\mu$g). |
| $Lp$ | : Water conductivity ($\mu$m/s/kPa). |
| $Ml_s^e, Ml_s^i$ | : Molality of external and internal permeable solutes (mol/kg $H_2O$). |
| $Ml_n^e, Ml_n^i$ | : Molality of external and internal non-permeable solutes (mol/kg $H_2O$). |
| $m$ | : Mass of the solution ($\mu$g). |
| $m_i$ | : Mass of the solute $i$ ($\mu$g). |
| $m_w$ | : Mass of water ($\mu$g). |
| $N$ | : Avogadro's number (mol$^{-1}$). |
| $P_s$ | : Permeability of solute ($\mu$m/s). |
| $r_i$ | : Molecular radius of solute $i$ (mm). |
| $R$ | : Universal gas constant (J/mol/K). |
| $S$ | : Exchange area (mm$^2$). |
| $Sc$ | : Cell area ($\mu$m$^2$). |
| $t$ | : Time (s). |
| $T$ | : Temperature (K). |
| $V(t)$ | : Cell volume ($\mu$m$^3$). |
| $Vb$ | : Osmotically inactive cell volume ($\mu$m$^3$). |
| $\overline{V_s}$ | : Partial volume of solute s (L/mol). |
| $x$ | : Co-ordinate (mm). |
| $\eta$ | : Dynamic viscosity of the solution ($\mu$g/mm/s). |
| $\lambda$ | : Thermal conductivity coefficient (W/mm/K). |
| $\sigma$ | : Reflexion coefficient (without units). |

## 1. INTRODUCTION

Sperm cryopreservation must guarantee high cell viability to be accepted as a breeding tool. Viability is affected by extender composition, temperature protocol, container and individual freezing ability [16, 40–46]. Since these parameters are too numerous to be tested rapidly and because unbiased experiments on rapid phenomena are difficult to set up, mathematical models can complement experimental work [11, 18, 20–24, 29–31, 35, 37, 44, 45]. Most published numerical models describe only a part of the phenomena or one step in the technique. Of course, incomplete models can be enriched by experiments, and discordances between field results and theories [11, 13] have already led to the discovery of new biological properties and structures [12]. However, when models concern only a part of the technique, they hardly integrate previously built cell histories and equilibria.

We have developed a numerical simulation mastering most physical, chemical and biological parameters occurring during all steps of the technique. We compared the calculated results to those obtained with electron microscopy of cells located at different depths in straws and bags and to results published in the literature [3, 4, 15, 16, 42]. The aim was to predict rapidly cell viabilities at each step of the technique, from ejaculation to thawing, with a final error lower than 10%. The physical part of the model concerns the calculation of temperatures at different times and depths in the cryocontainer, taking into account that the thermal balance is imposed externally by gas/liquid baths or thermal machines and internally by conduction and mass diffusions. The chemical part concerns the phase transitions and extender physico-chemical modifications. The extenders may include the usual salts and saccharides, buffers, permeable cryoprotective agents (CPA), egg yolk, skimmed milk and emulsifiers. Their compositions can be changed sequentially, to simulate dilutions, additions or replacement of components during the steps of the technique. The biological part includes calculations of cell volumes and surfaces, intracellular water, ice, salts and CPA, as well as an evaluation of four common cell injuries. When the simulations were first used for validation, it appeared that several new parameters had to be added to fit with experimental data. This led us to introduce both the concept of molecular chicanes, explaining the limited water diffusions in concentrated solutions, and a multi-compartment cell model with species-specific geometry and properties.

## 2. MATERIAL AND METHODS

### 2.1. Containers and plastic properties

Flat plastic bags or cylindrical straws of different sizes were simulated. The density, heat mass, heat conductivity and their variations with temperature

were obtained by interpolations between table values [25] or from polynomial regressions.

### 2.2. Thermal and mass transfers

The containers being symmetrical, only half of the geometrical domain needed to be calculated. This domain, including the extender and the container wall, was separated into $n$ layers stacked from the center to the periphery. The layers were parallelepipeds for bags, or concentric torre sectors for straws. The thermal conduction and the mass diffusion in any layer and for any component of the extender indexed as $i$ were calculated from Fourier's and Fick's laws (1 and 2).

$$m(x)c\frac{\partial T(x,t)}{\partial t} = -\lambda(x)S(x)\frac{\partial T(x,t)}{\partial x} + \lambda(x+\mathrm{d}x)S(x+\mathrm{d}x)\frac{\partial T(x+\mathrm{d}x,t)}{\partial x} \quad (1)$$

$$\frac{\partial m_i(x,t)}{\partial t} = -D_i(x)S(x)\frac{\partial c_i(x,t)}{\partial x} + D_i(x+\mathrm{d}x)S(x+\mathrm{d}x)\frac{\partial c_i(x+\mathrm{d}x,t)}{\partial x} \quad (2)$$

The diffusivity coefficient ($D$) of any solute ($i$) displaying a molecular radius $r$ was obtained by the Stokes-Einstein [28] equation (3).

$$D_i = \frac{RT}{6N\pi\eta r_i}\cdot \quad (3)$$

Equations (1 and 2) were discretized, following the implicit scheme (4), with finite differences, constant spaces and time steps. In this scheme, $X_k$ represents either the temperature or the mass of the solute ($i$) in the layer ($k$).

$$a_x X_{k-1} + b_k X_k + c_k X_{k+1} = f_k \qquad k = 1, ..., n. \quad (4)$$

The temperature on the external side of the container being imposed by the cooling/warming system, no mass diffusion occurs in the plastic and no mass or thermal diffusion occurs in the center. Therefore, $f_n = 0$, $c_n = 0$ and, $a_1 = 0$. The resulting scalar tridiagonal system was solved using the Thomas algorithm [27].

### 2.3. Water/ice phase transition

#### *2.3.1. Melting temperature*

The local melting and eutectic temperatures were calculated with one of the Pegg algorithms [35, 36] according to the CPA in use. Since they apply only to solutions containing water, NaCl and CPA, we determined the osmosity (an NaCl concentration with similar thermodynamic properties) for each other solute from [25]. An equivalent NaCl concentration was then obtained from the sum of osmosities and the reverse osmosity table for NaCl [25].

#### 2.3.2. *Phase transitions*

The melting and eutectic temperatures indicate whether a phase transition is possible. When applicable, the difference between local and melting temperatures ($\Delta T$) was converted into a mass of water or ice $\Delta m_w$, a function of the latent heat of fusion ($L$). The latter, which varies for temperatures higher than 171 K, was determined from a third-order polynomial refinement of the Kirchhoff law (5) [43].

$$L\Delta m_w = mc\Delta T. \tag{5}$$

When two phases coexisted, the local temperature was forced to equal the melting temperature.

#### 2.3.3. *End of crystalline ice formation in extender and cells*

For each layer, three criteria were used to limit large ice crystals growing or melting:

- the first dynamic threshold was the temperature of the eutectic phase, under which the crystals stopped growing. Below, small crystals or vitreous ice are probably produced without expense of latent heat [43];
- the second limit was a percolation coefficient (liquid mass / total mass). Under 0.16, and for any 3D volume, the remnant liquids are considered not to be mobile enough to feed the surrounding ice crystals [32,43]. The remaining water can eventually be converted to vitreous ice;
- intracellular crystallization was also stopped when intracellular CPA concentration (w/w) exceeded 40% [1,2]. This last condition is not totally valid in vitrification protocols, but vitrification is not used for spermatozoa.

These three limits were calculated without priority. Crystal growth or melting was stopped as long as one of the conditions above occurred in the layer.

### 2.4. Calculation of equation coefficients and extender modifications

Most of the equation parameters are sensitive to temperature and/or concentrations. For each extender component, the dynamic viscosities, densities, thermal conductions, and specific heats were calculated using polynomial determinations or interpolation between values of tables. The volume and size of the layers were recalculated at each time step from densities and mass balance after diffusion. For bags, variations in volumes were reported in terms of thickness because commercial plastic bags support expansion in this direction. For straws, volume variations were reported in terms of length, since one air bubble is usually left close to the tip to buffer any pressure variation. The physical properties of egg yolk were obtained from [10,33,34,39] and the fractions of

**Table I.** Final cell status after simulation of freeze-thawing of boar spermatozoa, in lactose (11%) egg yolk (20%) extender containing 3% glycerol, with or without OEP, frozen at −55 °C/min and thawed at +50 °C in 0.5 ml PVC straw.

| | With OEP | Without OEP | Difference |
|---|---|---|---|
| Intact cells | 36.59% | 28.44% | 8.15% |
| salted | **10.16%** | **18.81%** | **8.65%** |
| broken | 2.21% | 1.72% | −0.49% |
| iced | 51.02% | 51.02% | 0.00% |

sugars bound to egg yolk [33], or salts to proteins [26] were not recorded as solutes.

When "orvus es paste" (OEP), is added to extenders containing egg-yolk, a micro-emulsion with higher viscosity is formed and 5 to 8% more living boar spermatozoa can be recovered. The viscosity of micro-emulsified egg-yolk not being documented, we set this parameter semi-empirically until experimental [17] and simulated results were similar (Tab. I). This is achieved by a close to 5-fold increase in egg-yolk viscosity. Under these conditions, the simulations showed that mass diffusions between layers were limited and that extender concentrations and cell volumes remained more homogeneous at different depths.

### 2.5. Variations in cell volume

Cell volumes and surfaces were calculated with the Kedem and Katchalsky equations describing mass transport of water and permeable solutes through cell membranes, as described in [24]:

$$\frac{\mathrm{d}V}{\mathrm{d}t} = LpScRT\left[\left(Ml_n^i - Ml_n^e\right) + \sigma\left(Ml_s^i - Ml_s^e\right)\right]. \tag{6}$$

The variations in intracellular permeable solutes were determined according to:

$$\frac{\mathrm{d}lMl_s^i}{\mathrm{d}t} = \frac{\left(1+\overline{V}_s Ml_s^i\right)^2}{V - V_b} \times \left\{\left[\overline{Ml}_s(1-\sigma) - \frac{Ml_s^i}{1+\overline{V}_s Ml_s^i}\right]\frac{\mathrm{d}V}{\mathrm{d}t} + ScPs\left[\left(Ml_s^e - Ml_s^i\right)\right]\right\} \tag{7}$$

$$\text{with} \quad \overline{Ml}_s = \frac{Ml_s^e - Ml_s^i}{\left(\ln Ml_s^e - \ln Ml_s^i\right)}.$$

The activation energies associated with water and CPA transports were applied to (8) for temperature correction. The reflexion coefficient $\sigma$ (9) regulates

**Table II.** Geometric model used for mammalian spermatozoa. They are likened to a parallelepiped (head) and two cylinders (mid piece and main piece). Values are in $\mu$m, $\mu m^2$ and $\mu m^3$ corresponding to the isoosmotic equilibrium. For each part, the minimal volume is equal to the dry volume and * only one dimension is variable.

| Species | Head | | | Mid piece | | Main piece | | Total |
|---|---|---|---|---|---|---|---|---|
| | Length | Width | Thickness* | Length | Radius* | Length | Radius* | Volume / Area |
| Ram | 8 | 4.5 | 0.42 | 12 | 0.59 | 20 | 0.1 | 31.0 / 139 |
| Boar | 7 | 4.5 | 0.25 | 20 | 0.45 | 23 | 0.281 | 26.3 / 156 |

the simultaneous or independent transport of water/CPA and/or the frictions during the transport through plasma membranes.

$$P_a(T) = P_{a0} \cdot \exp\left([Ea/R]\,[1/T_0 - 1/T]\right) \tag{8}$$

$$\sigma = 1 - \left(P_s \overline{V}_s\right)/RTLp. \tag{9}$$

### *2.5.1. Cell model*

The variations in cell volume were redistributed into three compartments (head, mid-piece and main-piece) weighted by their respective surfaces (Tab. II). The volume of each compartment was never allowed to be lower than the dry volume. The head was considered as a parallelepiped of variable thickness. The mid- and main-pieces of the flagellum were likened to cylinders of variable radius. The surfaces were recalculated accordingly.

### *2.5.2. Modifications in trans-membrane water transport by molecular chicanes and mobility of liquid water*

The equations (6–9) allow calculation of volumes and intracellular concentrations in cells surrounded by simple extenders (water, salts, CPA). In more complex media [24] and at low temperatures [13, 37], variations in volume are lower than predicted by the model. This could be due to the binding of egg yolk and/or other components to plasma membranes as observed earlier [6]. This binding constitutes an additional barrier to transport through biological membranes. For this reason, we modulated the cell volume variations due to water diffusion by a coefficient $\alpha$ = mass of liquid water/mass of the liquid or mushy phase in the layer.

This coefficient is independent of the extender composition and refers to the number of $H_2O$ molecules likely to access a plasma membrane before passing through it. This opportunity diminishes when the cells immediate surroundings become crowded with non-aqueous molecules playing the role of chicanes.

Water transport through plasma membranes was also stopped when the local percolation coefficient for water was lower than 0.16. For reasons similar

to those presented above (Sect. 2.3.3), when water molecules are not mobile enough to feed ice crystals, they cannot move towards plasma membranes.

### 2.6. Prediction of cell injuries

We consider that only large intracellular crystals are deleterious to cells and that frozen cells are insensitive to changes in osmolarity. Four criteria were used:

- Solution effect or salting out
  In the boar and the ram, the maximum admitted intracellular salt concentration in water + CPA (W/V) was set at 30% [45]. Above this concentration, 0.4% (ram) or 0.1% (boar) of the cells were killed per second.
- Cell swelling and stretching of membranes
  To simulate osmotic lysis, resulting in cell viabilities similar to measurements made in the boar [24] and the ram [11, 44], we used a stretching threshold and a maximum admitted cell volume (Fig. 1). These limits were applied to the plasma membranes covering any cell compartment.
  Above the stretching threshold STH ($\mu m^2/s$), X%$s^{-1}$ cells were killed. In the boar, STH = 1.6 and $X = 14$. In the ram, the temperature dependency of membrane weakness is known [11]. Therefore, STH was fixed at 11.5 at 30 °C and 7.5 at 18 °C or lower temperatures. Linear interpolations were used for intermediate temperatures and $X = 1$.
  Above the maximum cell volume MCV ($\mu m^3$), Y% cells were destroyed per second. MCV = 34 and $Y = 2.6$ in the boar while MCV= 62 and $Y = 12$ in the ram.
- Dissection by ice
  Cell dissection was calculated only when large ice crystals growth has stopped. The cells were considered injured when intracellular crystalline ice was higher than 30% of the isotonic volume.

### 2.7. Electron microscopy of frozen samples and viability after thawing

Ram spermatozoa were frozen in 0.5 ml PVC (polyvinyl chloride, 2.4 mm internal diameter) straws following the protocol devised in [5] and after dilution in either extender A (10% egg yolk +4% skimmed dry milk +4% glycerol +8% lactose in water) or extender B (20% egg yolk +4% glycerol +7% lactose). Glycerol was added at 4 °C and the straws were frozen at −1 K/s over liquid nitrogen vapors before being stored at −196 °C.

After several days, frozen straws were cut at −196 °C into 3 mm long pieces which were cryofixed and cryosubstituted for 3 days at −80 °C with 2% osmium tetroxide in acetone before being warmed to room temperature [6, 38]. After

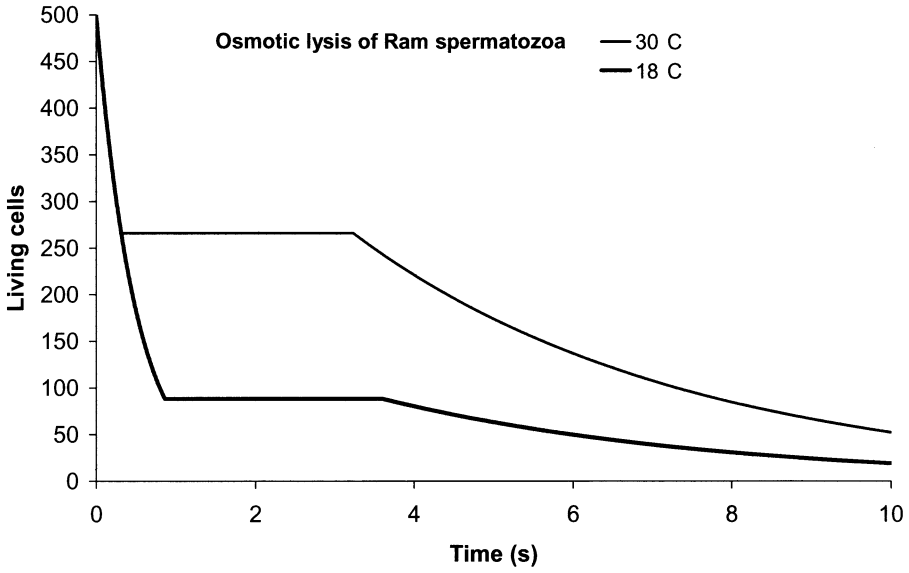


**Figure 1.** Osmotic lysis of ram spermatozoa. When ram spermatozoa are subjected to a hypo-osmotic shock, from 300 to 30 mOs/Kg$H_20$, the number of living cells decreases dramatically within 1 second due to rapid stretching of the plasma membranes. After a plateau which corresponds to intake of water by the cells, the maximum cell volume limit is exceeded, and the cell number continues to decrease. The cells are more sensitive to stretching at 18 °C than at 30 °C. The parameters used to draw the curve and simulate the phenomenon were obtained semi-empirically to mimic the Curry and Watson results [11].

3 washes in acetone at 20 °C, samples were embedded in EPON resin, and cured at 50 °C. The ultra-thin sections placed on electron microscopy grids were stained with uranyl acetate and lead citrate and observed in a Philips EM400 electron microscope. Scaling from external to internal parts of the straws made use of the known interval between grid bars.

The dead cells were checked by staining of smears with eosin/nigrosin 5 min after thawing of sister straws at 50 °C for 1 min.

## 3. RESULTS

### 3.1. Electron microscopy and simulations in ram spermatozoa

#### *3.1.1. Electron microscopy and viability in 0.5 ml PVC straws*

Using protocol A (Lactose-egg yolk, milk) no intracellular ice was observed in cells located close to the straw wall (Fig. 2a). In cells located 0.3 – 0.9 mm from the periphery (Figs. 2b and 2c), ice was present in and outside acrosomes.

Most acrosomes were destroyed in the center of the straw (0.9 to 1.2 mm, Fig. 2d).

Using protocol B (lactose-egg yolk), many cells at the immediate proximity of the plastic were dehydrated. Ice was evident around most flagella (Fig. 2e). The cells located between 0.3 and 0.6 mm from the wall generally displayed few defects (Fig. 2f). Ice was present in some acrosomes located between 0.6 and 0.9 mm (Fig. 2g) and the cells in the center were destroyed (Fig. 2h).

#### *3.1.2. Simulation of freeze-thawing ram spermatozoa with protocols A and B*

The simulated living cell ratios (35 and 48% respectively after protocols A and B) were close from the 33 and 50% undamaged spermatozoa recorded by vital staining (Tab. III). The difference between protocols mostly resulted from stretching of plasma membranes during thawing in extender A. In the latter, the viscosity was low, and the glycerol concentrations rapidly decreased by dilution in the most peripheral layers during thawing. This resulted in a rapid variation in cell volume [24].

### 3.2. Simulation of freeze-thawing protocols for the boar

**3.2.1.** The cryopreservation of boar spermatozoa in 0.5 ml PVC straws devised by Thilmant [42] results in excellent prolificacy. Only 7% of the cells are lost. When compared to other methods, the extender is rich in egg yolk (22.6%) and the freezing step follows a long stay of the straws at −4.5 °C. The simulation produced similar results (Tab. IV) and revealed where and when the cells were injured: no physical damage occurred prior to freezing. Few cells (2.77%) were ice-damaged in the most central part of the straw during cooling from −4.5 °C to −40 °C, and 6.91% more cells displayed membrane stretching damage during the redilution in BTS (Beltsville Thawing Solution) after thawing, due to the one-step removal of glycerol.

**3.2.2.** The three cooling/thawing protocols applied to three different containers devised by Bwanga *et al.* [3, 4] were simulated (Tab. V). The overall mean error in simulations was close to 1.6%. Individual errors remained lower than 10% for flat bags. This large difference can be explained by the use of Teflon flat bags by Bwanga *et al.* [4]. Since their density and thermal properties were unknown, we simulated PVC instead.

## 4. DISCUSSION

A numerical simulation using nested equations, solving thermal, physical, chemical and cellular changes during all steps of freezing/thawing of spermatozoa, predicts cell viability with a mean error below 5% in the ram and the

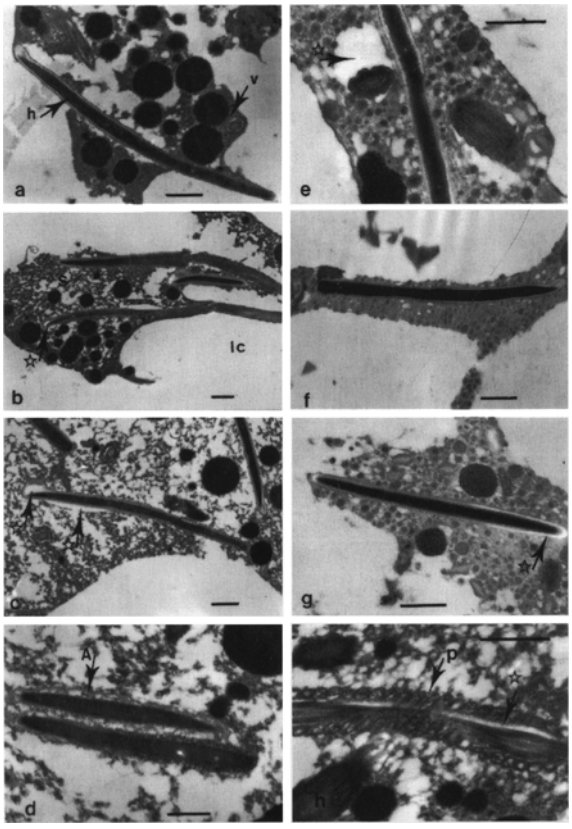


**Figure 2.** Electron microscopy of cryosubstituted ram spermatozoa frozen in 0.5 ml PVC straws. Spermatozoa frozen with protocol A (milk-egg yolk extender, a, b, c, d) and protocol B (egg-yolk extender, e, f, g, h). Bars = 1 $\mu$m. a and e) from the inner straw wall to 0.3 mm, b and f) from 0.3 to 0.6 mm, c and g) from 0.6 to 0.9 mm, d and f) from 0.9 to 1.2 mm (the center of the frozen material). a) Most spermatozoa (h = head) are located in veins (v) of concentrated extender separating large ice crystals (white areas). b) Ice (☆) is present at the tip of the sperm head, under the acrosomes. Small ice crystals (s) are present in veins surrounded by large crystals (lc). c) More intracellular ice (☆) is present under the acrosomes and between the acrosomes and the plasma membranes of spermatozoa. Many small crystals are present in the extender. d) All acrosomes (A) are destroyed in the center of the straw. The center is filled with ice and extender. The latter is less organized than at the periphery. The veins are not well defined. e) The cells are strongly dehydrated. No ice is present in heads and most flagella are surrounded by ice shadows(☆), suggesting that their original volume was larger, before being dehydrated. f) The extender contains very few ice crystals. No ice is observed in cells. g) More ice crystals are seen in the veins of extender, and ice (☆) is present in acrosomes. h) Same situation as in Figure 2d: Mid piece of a frozen spermatozoon. In the center of the straw, ice and extender are mixed and cells are filled with ice crystals (☆) while the plasma membrane (p) is destroyed.

**Table III.** Cell states in the three steps where ram spermatozoa damage is predicted in simulations with extenders A (egg-yolk + milk) and B (egg-yolk). Protocols A and B were also used for electron microscopy. Layers 1 to 6 refer to the center to periphery of 0.5 ml PVC straws. Percentages and means are rounded of respectively 0 to 2 decimals. Value = 0 means that the value was changed due to the technique. Missing values mean that no change occurred. Both protocols result in numerous cells that are ice-damaged in the center. Extender A is better during the freezing step (fewer cells are salted out). Similar salting ranges are predicted for both protocols during thawing. The disadvantage of protocol A appears during thawing and redilution owing to membrane ruptures. At these steps, the ruptures are provoked by a rapid area variation in cells following fast intracellular glycerol removal.

| | | Protocol A | | | | Protocol B | | | |
|---|---|---|---|---|---|---|---|---|---|
| Step | Layer | Intact | Salted | Broken | Iced | Intact | Salted | Broken | Iced |
| Freezing | | % | % | % | % | % | % | % | % |
| | 1 | 0 | | | 100 | 0 | | | 100 |
| | 2 | 0 | 10 | | 90 | 0 | | | 100 |
| | 3 | 0 | 10 | | 90 | 0 | | | 100 |
| | 4 | 97 | 3 | | | 100 | | | |
| | 5 | 100 | | | | 79 | 21 | | |
| | 6 | 100 | | | | 74 | 26 | | |
| | **1-6** | **74.42** | **2.79** | | **22.77** | **62.05** | **12.94** | | **25** |
| Thawing | 1 | 0 | | | 100 | 0 | | | 100 |
| | 2 | 0 | 10 | | 90 | 0 | | | 100 |
| | 3 | 0 | 10 | | 90 | 0 | | | 100 |
| | 4 | 73 | 3 | 24 | | 100 | | | |
| | 5 | 78 | | 22 | | 64 | 36 | | |
| | 6 | 38 | 62 | | | 60 | 40 | | |
| | **1-6** | **45.17** | **21.68** | **10.36** | **22.77** | **53.98** | **21.01** | | **25** |
| Redilution | 1 | 0 | | | 100 | 0 | | | 100 |
| | 2 | 0 | 10 | | 90 | 0 | | | 100 |
| | 3 | 0 | 10 | | 90 | 0 | | | 100 |
| | 4 | 56 | 3 | 41 | | 90 | | 10 | |
| | 5 | 60 | | 40 | | 58 | 36 | 6 | |
| | 6 | 29 | 62 | 9 | | 54 | 40 | 6 | |
| | **1-6** | **35.02** | **21.68** | **20.51** | **22.77** | **48.58** | **21.02** | **5.39** | **25** |

**Table IV.** Summary of final results generated by the numerical simulation of the Thilmant protocol. Most cell damage occurs after thawing. Simulations and field results (total number of living cells) are close.

| | N | % |
|---|---|---|
| Total Cells | 1000000 | 100.00 |
| Ice damage | 27778 | 2.77 |
| Salted out | 0 | 0.00 |
| Exploded | 0 | 0.00 |
| Damaged membranes | 68927 | 6.89 |
| Intact Cells | 903295 | 90.32 |

**Table V.** Comparison of living cells (observed motile % *versus* simulated uninjured %) after simulation of the three Bwanga *et al.* [3, 4] protocols. Briefly, in protocol A, the cells are cooled from 5 °C to −6 °C (−3 °C/min) and are left at −6 °C for 1 min before being frozen (−20 °C/min). In protocol B the cells are cooled from 5 °C to −6 °C (−3 °C/min) before being frozen (−30 °C/min). In protocol C, the cells are frozen rapidly: 5 °C to −100 °C at −35 °C/min. For all protocols, thawing is done in water baths (50 °C).

| Protocol | A observed | Simulated & (difference) | B observed | Simulated & (difference) | C observed | Simulated & (difference) |
|---|---|---|---|---|---|---|
| Straw 0.5 | 52 | **54** (+2) | 36 | **41** (+5) | 25 | **31** (+6) |
| Straw 5 ml | 29 | **28** (−1) | 20 | **20** (0) | 13 | **14** (+1) |
| Flat bag | 55 | **46** (−9) | 36 | **34** (−2) | 22 | **32** (+10) |

boar. In addition to field experiments, the simulations explain where, when and why cells are affected.

### 4.1. Thermal exchanges

The equations above are valid if the extender is not subjected to pressure. In fact, straws ordinarily contain air bubbles to absorb over-pressures, and bags are generally soft enough to support dilatations without opposing strong resistance. Only the diffusion fluxes occurring in the smallest dimension, the thickness of bags or the diameter of straws, are calculated here. Since exchanges in other directions, border effects and gravity are neglected, the thermal and mass transfer calculations apply to a mean slice in the container. The model is not valid for cubic or spherical containers. Due to the low ratio between the smallest dimension/any other dimension in bags or straws, the error for estimated temperature should be low. In fact, a thawing temperature variation recorded as 1443 K/min [42] is simulated as 1423 K/min (1.38% difference). When Bwanga protocols [3] are simulated, the calculated and recorded temperatures curves are also close.

### 4.2. Thermodynamic properties of the extender

The properties of the extender components vary with concentration and temperature. Thermodynamic values cannot be calculated through simple equations because ideality of solutions is lost as they concentrate. For this reason, many parameters were obtained by interpolation from tables.

Concentration also results in modification of the hydration shells around solute molecules and changes their thermodynamic properties. This problem was solved here by using the osmosity of each solute. Osmosity integrates the interactions of the solute with the solvent and with sister molecules. Since the known interactions between sugars, salts, milk and egg yolk were calculated separately, we believe that the most necessary precautions have been taken to describe mathematically the extender. Thanks to Pegg's equations [35,36], freezing and eutectic temperatures can be calculated for a three-components solution (water, NaCl and CPA). For more complex extenders, the NaCl concentration in Pegg's equations was replaced by a calculated NaCl equivalent explaining the thermodynamic properties of all solutes but CPA. When using this procedure, the calculated freezing point depression and osmolalities of more than 20 standard extenders were similar to measurements, and the freezing point depressions of simple solutions containing sugars or CPA were also similar to records [19].

### 4.3. Start and end of ice formation in extender and cells

It is a common observation that the temperature increases prior to the initial formation of ice, due to delayed ice crystallization and release of latent heat of fusion [3]. Ice crystals need an ice surface to grow properly. As long as the first crystal has not nucleated, water is in a super-cooled phase. In the present work, we did not calculate the curvature of crystals and the energy needed to feed them. This would have resulted in calculations too lengthy to be compatible with the aim of the project. However, we have evaluated the risk: (1) since the beginning of ice formation is predicted slightly earlier, the concentration of the extender and the cell dehydration also start earlier. Therefore, intracellular ice formation is delayed and the calculated global cell vitality is essentially unaffected. (2) The release of latent heat of fusion not being calculated, the lowering of temperature and the initial crystal growth are slowed down in simulations. This counterbalances early crystal initiation. When comparing published and simulated temperature curves, the error in overall freezing speed remained lower than 2%.

Since we consider that only crystalline ice is deleterious to cells [30,31], the end of crystallization needs to be evaluated. Growing of crystals becomes difficult at low temperature due to high CPA and increased salt concentrations [19,32,35,36]. The high viscosity in the eutectic phase implies that the unfrozen liquids do not move easily towards the surface of large crystals. This

phenomenon is commonly observed with electron microscopy of frozen samples. Spermatozoa are generally embedded in layers of concentrated extender surrounding large crystals. The layers contain clear micro-areas which could represent either vitreous ice or micro-crystals [6]. Their amount varies with the extender composition, the freezing speed and the depth in containers [16]. The three limits used in our simulations (eutectic temperature, percolation coefficient and CPA concentration) are largely validated in the literature [1,32,35,43].

### 4.4. Cell volumes/surface and cell damage

- Cell volume and surface
  Variations in the volume of spermatozoa during freezing and thawing are mainly driven by the specific water ($Lp$) and CPA ($L_s$) permeabilities, the values of which vary according to the measurement technique [11] and the extender composition. For experimental convenience, $Lp$ are generally determined in simple mineral solutions and at temperatures above 273 K. In the presence of macromolecules, $Lp$ can be lowered by 40% [24]. For these reasons, calculations do not always fit with field experiments [11–13]. This was the case here with our first simulations. To refine the model, we have introduced the concept of molecular chicanes, made of solute molecules located close to the plasma membrane. They act as barriers that water molecules must pass around before meeting the membranes. Actually, macromolecules such as egg-yolk components are bound to plasma membranes [6]. The chicanes modulate Lp dynamically following the progressive rarity of liquid water when ice mass and solute concentrations increase. This new condition allows reconciliation of the model with experiments using various extenders [3,4,6–9,15–17,42].
- Cell damages
  If biological hazards are ignored, most possible remaining damage is related to physical changes induced by the technique. Damages can be reduced to four types: dissection by intracellular ice, cell dryness, membrane stretching and incursion of liquids into cells. We evaluate the quantity of intracellular ice following several hypotheses:
  1) the formations of crystalline or vitreous ice are directed by the same laws inside or outside the cells. Ice crystal formation could be delayed in large cells [30], but probably not in spermatozoa, thanks to their small dimensions;
  2) the water involved in molecular hydration shells is limited to 30% of the cell dry mass as demonstrated in [7,14,32];
  3) the 40% CPA concentration is admitted as a threshold above which vitreous ice is the main type formed [1,2]. Of course, some crystals could be formed with higher CPA concentration and fast cooling speed [31], but in classical sperm freezing protocols, crystalline ice

growth generally stops before the CPA concentration reaches such values.

Our evaluation of intracellular ice mass is clearly an over-simplification because spermatozoa display complex shapes and sub-cellular compartments filled with heterogeneous organelles. However, the calculated cell injuries are similar to those observed by electron microscopy in the depth of frozen material, both in the boar [7,8,15,16] and in the ram.

In our simulations, cell swelling due to exceeding cell volumes are rare. In the excellent technique developed by Thilmant for freezing boar spermatozoa [42], simulations classify stretching as the main deleterious effect, once intracellular crystallization and solution effects have been perfectly mastered. These excellent results can be attributed to an extender with a high viscosity (OEP + egg yolk) which limits diffusion, thus homogenizing the cell osmotic responses. The second original step is a long stay of the straws at $-4.5$ °C. During this step, the simulation shows that thin ice dendrites are formed in the extender running from the straw wall to the center. Since this initial ice growth is limited, no marked concentration of the extender is observed. However, heat conduction of ice being greater than that of liquid water, the thin dendrites act as heat exchangers during the real freezing step. Changes in temperature, ice mass, osmolality and cell areas are quite homogeneous in the different layers during freezing and thawing. In protocols killing more cells, stretching often affects cells located away from both the plastic wall and the container center. This is common in most techniques using 5 ml straws [15]. The four parameters set to calculate cell swelling clearly confirm that: (1) the membrane stretching and (2) a maximum limit in cell volume, are sequentially involved in osmotic shocks [11]. The parameters defined here for temperature above 30 °C (boar) and 18 °C (ram) could need refinements, due to increased membrane stiffness at low temperature. However, the stretching limit above which cells are affected is self-regulated during freezing. As dehydration progresses, the cell area is reduced and area variations become limited.

### 4.5. Conclusions and applications

The simulation program built to evaluate spermatozoa ability to survive cryopreservation is validated in the boar and the ram. In these species, it predicts where, when, why and how several cell injuries occur with acceptable errors. Many more simulations than those presented here have been conducted. They reveal that 5 to 15% cell losses before freezing and/or after thawing are quite common. These steps probably need some attention. For instance, the composition of the extender used for dilutions after thawing is very critical. The addition of CPA has also been claimed as a large source of problems. Simulations show that it can be overcame by a judicious extender composition. However, this facility can be counterbalanced by a more critical CPA removal

during thawing. Simulations help in finding compromises. While damage occurring during the freezing steps can be controlled by appropriate extenders and/or cooling rate protocols, thawing of closed containers can only be monitored through the warming protocol. Therefore, choosing an appropriate extender is essential. In addition to being non-toxic, life-supporting, pH-buffered and carrying cell energy substrates, the extender must offer other specific properties. Whatever the cooling protocol, and due to the percolation threshold, its final osmolality will never be multiplied by more than 6.25 during freezing. Cells must support such changes and withstand the speed of variation. This indicates that the cooling and warming speeds are the second and third important factors. The dynamic viscosity of the extender also facilitates or limits the diffusion of solutes. This parameter can be fixed to reduce heterogeneities in cell hydration in the depth of the cryo-container when adapted in combination with specific temperature protocols. However, for large containers, it remains difficult to solve the double problem of cell dehydration (mostly) at the container periphery and ice damage in the center. In this situation, numerical simulations allow the choice of a "window" with optimal number of potentially living cells.

The main conclusions drawn from the present work are the following: (1) physical, chemical and cellular parameters interact and small modifications in any parameter can lead to dramatic effects. (2) Steps of the technique cannot be "isolated". All steps interfere sequentially. (3) Since cell volumes and surfaces are monitored through specific water and CPA permeabilities, general advice concerning extenders and temperature protocols cannot be ruled out independently of the species.

## ACKNOWLEDGEMENTS

This work was granted by the *Bureau des Ressources Génétiques*, Paris, France. We thank Y. Guérin for collection of ram semen, J.C. Nicolle and A. Begué for photographic work, H. Bosc for help in collecting bibliography. The models in the boar and the ram were validated thanks to data published by C.O. Bwanga, G. Colas, P. Guillouet, H. Ekwall, W.M.C. Maxwell, M. Paquignon, S. Salamon and P. Thilmant.

## REFERENCES

[1] Boutron P., Comparison with the theory of the kinetics and extent of ice crystallization and the glass-forming tendency in aqueous cryoprotective solutions, Cryobiology 23 (1986) 88–102.

[2] Boutron P., Kaufmann A., Stability of the amorphous state in the system water-glycerol-dimethylsulfoxide, Cryobiology 15 (1978) 93–108.

[3] Bwanga C.O., De Braganga M.M., Einarson S., Rodriguez-Martinez H., Cryopreservation of boar semen in mini- and maxi-straws, J. Vet. Med. A 37 (1990) 651–658.

[4] Bwanga C.O., Einarson S., Rodriguez-Martinez H., Cryopreservation of boar semen. II -Effect of cooling rate and duration of freezing point plateau on boar semen frozen in mini- and maxi-straws and plastic bags, Acta Vet. Scand. 32 (1991) 455–461.

[5] Colas G., Effect of initial freezing temperature, addition of glycerol and dilution on the survival and fertilizing ability of deep-frozen ram semen, J. Reprod. Fertil. 42 (1975) 277–285.

[6] Courtens J.L., Paquignon M., Ultrastructure of fresh, frozen, and frozen-thawed spermatozoa of the boar, in: Johnson L.A., Larsson K. (Eds.), Deep freezing of boar semen, Swedish University of Agriculture, Uppsala, 1985, pp. 61–87.

[7] Courtens J.L., Ekwall H., Paquignon M., Plöen L., Preliminary study of water and some element contents in boar spermatozoa, before, during and after freezing, J. Reprod. Fertil. 87 (1989) 613–626.

[8] Courtens J.L., Paquignon M., Blaise F., Ekwall H., Plöen L., Nucleus of the boar spermatozoon: Structure and modifications in frozen, frozen-thawed, or sodium dodecyl sulfate-treated cell, Mol. Reprod. Dev. 1 (1989) 264–277.

[9] Courtens J.L., Theau-Clement M., Ultrastructural modifications of rabbit spermatozoa induced by two freezing and thawing techniques, In: Lebas F. (Ed.), Proceedings of the 6$^{th}$ World Rabbit Congress, Association Française de Cuniculture, 63370 Lempdes, France, 1996, Vol. 2, pp. 59–63.

[10] Cunningham F.E., Viscosity and functional ability of diluted egg yolk, J. Milk Food Technol. 35 (1972) 615–617.

[11] Curry M.R., Millar J.D., Watson P.F., Calculated optimal cooling rates for ram and human sperm cryopreservation fail to conform with empirical observations, Biol. Reprod. 51 (1994) 1014–1021.

[12] Curry M.R., Millar J.D., Watson P.F., The presence of water channel proteins in ram and human sperm membranes, J. Reprod. Fertil. 104 (1995) 297–303.

[13] Devireddy R.V., Swanlund D.J., Roberts K.P., Bischof J.V., Subzero water permeability parameters of mouse spermatozoa in the presence of extracellular ice and cryoprotective agents, Biol. Reprod. 61 (1999) 764–775.

[14] Ekwall H., Plöen L., Courtens J.L., Embedding resin space, water contents and chromatin compaction in rabbit sperm nuclei: Electron microscopic X-ray spectrophotometry of a brominated probe, Andrologia 27 (1995) 175–184.

[15] Ekwall H., Erikson B., Courtens J.L., Rodriguez-Martinez H., Assessment of ice content and morphological alterations in boar spermatozoa frozen in maxi-straws, in: 13$^{th}$ Int. Congress on Animal Reproduction, ICAR, Sydney, 1996, Abst.

[16] Ekwall H., Eriksson B., Courtens J.L., Rodriguez-Martinez H., Ice granulometry and cell damages in boar semen frozen in two types of containers, Infusion therapy and Transfusionsmedizin 245 (1997) 29.

[17] Eriksson B., Ekwall H., Courtens J.L., Rodriguez-Martinez H., Effect of sodium dodecylsulphate on the frozen status and post-thaw viability of boar spermatozoa frozen in maxi-straws and plastic bags, in: 13$^{th}$ Int. Congress on Animal Reproduction, ICAR, Sydney, 1996, Abst.

[18] Fahy G.M., Levy D.I., Ali S.E., Some emerging principles underlying the physical properties, biological actions, and utility of vitrification solutions, Cryobiology 24 (1987) 196–213.

[19] Fullerton G.D., Keener C.R., Cameron I.L., Correction for solute/solvent interaction extends accurate freezing point depression theory to high concentration range, J. Biochem. Biophys. Methods 29 (1994) 217–235.

[20] Gao D.Y., Liu J., Mcgann L.E., Watson P.F., Kleinhans F.W., Mazur P., Critser E.S., Critser J.K., Prevention of osmotic injury to human spermatozoa during addition and removal of glycerol, Hum. Reprod. 10 (1995) 1109–1122.

[21] Gao D.Y., Mazur P., Critser J.K., Fundamental cryobiology of mammalian spermatozoa, in: Karow A.M., Critser J.K. (Eds.), Reproductive tissue banking, scientific principles, Academic Press, San Diego, London, Boston, New York, Sydney, Tokyo, Toronto, 1997, pp. 278–328.

[22] Gilmore J.A., McGann L.E., Liu J., Gao D.Y., Peter A.T., Kleinhans F.W., Critser J.K., Effect of cryoprotectant solutes on water permeability of human spermatozoa, Biol. Reprod. 53 (1995) 985–995.

[23] Gilmore J.A., Du J., Tao J., Peter A.T., Critser J.K., Osmotic properties of boar spermatozoa and their relevance to cryopreservation, J. Reprod. Fertil. 107 (1996) 87–95.

[24] Gilmore J.A., Liu J., Peter A.T., Critser J.K., Determination of plasma membrane characteristics of boar spermatozoa and their relevance to cryopreservation, Biol. Reprod. 58 (1998) 28–36.

[25] Handbook of Chemistry and Physics, $70^{\text{th}}$ edition, in: Weast R.C., Lide D.R.,. Melvin J.A., Beyer W.H. (Eds.), CRC Press, Boca Raton, FL, USA, 1990.

[26] Hardy J.J., Steinberg M.P., Interaction between sodium chloride and paracasein as determined by water sorption, J. Food Sci. 49 (1984) 127–131.

[27] Hirsch C., Thomas algorithm for tridiagonal systems, in: Numerical Computation of Internal and External Flows, Willey & Sons, Chichester, 1988, Vol. 1, pp. 505–508.

[28] Landau L.D., Lifshitz E.M., Fluid mechanics, in: Course of theoretical physics, Mir Publisher, Moscow, 1988, Vol. 6.

[29] Liu J., Wood E.J., Critser J.K., A theoretical approach to optimize interrupted-slow freezing protocol, in: Proceedings of the World Congress of Cryobiology, Marseille, France, 1999, Abst. 105.

[30] Mazur P., Freezing of living cells: Mechanisms and implications, Am. J. Physiol. 247 (1984) 125–142.

[31] Mazur P., Basic concepts in freezing cells, in: Johnson L.A., Larsson K. (Eds.), Deep freezing of boar semen, Proceedings of the $1^{\text{st}}$ Int. Conference on Deep freezing of Boar semen, Swedish University of Agricultural Sciences, Uppsala, 1985, pp. 91–111.

[32] Miller D.P., de Pablo J.J., Corti H., Thermophysical properties of trehalose and its concentrated aqueous solutions, Pharmacol. Res. 14 (1997) 578–590.

[33] Nau F., La congélation, in: Thapon J.L., Bourgeois M.C. (Eds.), L'œuf et les ovoproduits, Collection Sciences et Techniques Agro-alimentaires, Techniques et Documentation, Lavoisier, Paris, 1994, pp. 157–161.

[34] Palmer H.H., Ijichi K., Roff H., Redfern S., Sugared egg yolk: effects of pasteurization and freezing on performance and viscosity, Food Technol. 23 (1969) 85–108.

[35] Pegg D.E., Simple equations for obtaining melting points and eutectic temperatures for the ternary system glycerol/sodium chloride/water, Cryo-Letters 4 (1983) 259–268.
[36] Pegg D.E., Equations for obtaining melting points and eutectic temperatures for three ternary system dimethyl sulphoxide/sodium chloride/water, Cryo-Letters 7 (1986) 387–394.
[37] Phelps M.J., Liu J., Benson J.D., Willoughby C.E., Gilmore J.A., Critser J.K., Effects of percoll separation, cryoprotective agents, and temperature on plasma membrane permeability characteristics of murine spermatozoa and their relevance to cryopreservation, Biol. Reprod. 61 (1999) 1031–1041.
[38] Reger J.F., Escaig F., Pochon-Masson J., Fitzgerald M.E.C., Observation on crab, *Carcinus maenas*, spermatozoa following rapid freeze and conventional freezing technique, J. Ultrastruct. Res. 89 (1984) 12–22.
[39] Scalzo A.M., Dickerson R.W., Peeler J.T., Read R.B., The viscosity of egg and egg products, Food Technol. 24 (1970) 113–119.
[40] Schneider U., Mazur P., Osmotic consequences of cryoprotectant permeability and its relation to the survival of frozen-thawed embryos, Theriogenology 21 (1984) 68–79.
[41] Songasen N., Leibo S.P., Cryopreservation of mouse spermatozoa. II-Relationship between survival after cryopreservation and osmotic tolerance of spermatozoa from three strains of mice, Cryobiology 35 (1997) 255–269.
[42] Thilmant P., Congélation du sperme de verrat en paillette de 0,5 ml. Résultats sur le terrain, Ann. Méd. Vét. 141 (1997) 457–462.
[43] Viskanta R., Bianchi M.V.A., Critser J.K., Gao D., Solidification processes of solutions, Cryobiology 34 (1997) 348–362.
[44] Watson P.F., Recent development and concepts in the cryopreservation of spermatozoa and the assessment of their post-thawing function, Reprod. Fert. Dev. 7 (1995) 871–891.
[45] Watson P.F., Duncan A.E., Effect of salt concentration and unfrozen water fraction on the viability of slowly frozen ram spermatozoa, Cryobiology 25 (1988) 131–142.
[46] Woelders H., Matthijs A., Engel B., Effects of trehalose and sucrose, osmolality of the freezing medium, and cooling rate on viability and intactness of bull sperm after freezing and thawing, Cryobiology 35 (1997) 93–105.